Evaluation of an all sky imager based nowcasting system for distinct conditions and five sites

Cite as: AIP Conference Proceedings **2303**, 180006 (2020); https://doi.org/10.1063/5.0028670
Published Online: 11 December 2020

Bijan Nouri, Stefan Wilbert, Niklas Blum, Pascal Kuhn, Thomas Schmidt, Zeyad Yasser, Thomas Schmidt, Luis F. Zarzalejo, Francisco M. Lopes, Hugo G. Silva, Marion Schroedter-Homscheidt, Andreas Kazantzidis, Christian Raeder, Philippe Blanc, and Robert Pitz-Paal

Evaluation of an All Sky Imager Based Nowcasting System for Distinct Conditions and Five Sites

Bijan Nouri[1, a)], Stefan Wilbert[1], Niklas Blum[1], Pascal Kuhn[1], Thomas Schmidt[2], Zeyad Yasser[3], Thomas Schmidt[4], Luis F. Zarzalejo[5], Francisco M. Lopes[6], Hugo G. Silva[6], Marion Schroedter-Homscheidt[4], Andreas Kazantzidis[7], Christian Raeder[8], Philippe Blanc[9] and Robert Pitz-Paal[10]

[1]*German Aerospace Center (DLR), Institute of Solar Research, Ctra de Senes s/n km 4, 04200 Tabernas, Spain*
[2]*CSP Services GmbH, Friedrich-Ebert-Ufer 30, 51143 Cologne, Germany*
[3]*TSK Flagsol Engineering GmbH, Anna-Schneider-Steig 10, 50678 Cologne, Germany*
[4]*DLR, Institute of Networked Energy Systems, Carl-von-Ossietzky-Straße 15, 26129 Oldenburg, Germany*
[5]*CIEMAT Energy Department – Renewable Energy Division, Avda. Complutense 40, 28040 Madrid, Spain*
[6]*Renewable Energy Chair, University of Évora, Nossa Sra. da Tourega, 7000-083 Valverde, Évora, Portugal*
[7]*Laboratory of Atmospheric Physics, Department of Physics, University of Patras, 26500 Patras, Greece*
[8]*DLR, Institute of Solar Research, Prof.-Rehm-Str. 1, 52428 Jülich, Germany*
[9]*MINES ParisTech, 06904 Sophia Antipolis CEDEX, France*
[10]*DLR, Institute of Solar Research, Linder Höhe, 51147 Cologne, Germany*

[a)]Corresponding author: bijan.nouri@dlr.de

Abstract. All sky imager (ASI) based nowcasting system can provide spatially and temporally highly resolved solar irradiance information for the next minutes ahead. Nowcasts, which capture the intra-hour variability of the incoming downward shortwave solar irradiance, have the potential to optimize the operation of solar power plants as well as electrical grids. Such automatized optimizations require a deep understanding of the accuracy in the nowcasting system at any given moment. State of the art validation procedures of ASI based nowcasting systems use scalar error metrics without regards to the actual weather conditions. Yet, the performance of nowcasting systems varies strongly with the prevailing weather conditions. Deviations increase for more complex and variable conditions, for which it is more challenging to detect and model the clouds in the sky. Thus, depending on the used data set such validation results may not be meaningful to describe the expected accuracy in realistic and individual optimization situations. A novel validation procedure is presented in this work, which discretizes the validation data set in distinct temporal DNI variability classes. Individual error metrics are determined as function of the lead time and DNI variability class. This approach is applied for a two ASI based nowcasting system as operated on five distinct sites distributed in Spain, Portugal and Germany, over a combined period of more than 4.5 years. The obtained validation results emphasize that the novel classification method enables a comparison in nowcast performance between the sites despite of distinct local meteorological conditions. The presented method allows the estimation of the overall accuracy of nowcasting systems at a new site if DNI data in 1 min resolution are available.

INTRODUCTION

Direct normal irradiance (DNI) can be highly variable in space and time, even for small time intervals such as 15 min and within the area of a solar power plant. This spatial and temporal variability complicates the operation of concentrating solar power plants. For highly variable conditions, set temperatures might not be reached or even worse, they might be exceeded temporarily, which could cause emergency defocus incidents. Overall, such issues lead to a lower electricity production. Spatially resolved DNI information and its prediction for the next 15 min can

SolarPACES 2019
AIP Conf. Proc. 2303, 180006-1–180006-11; https://doi.org/10.1063/5.0028670
Published by AIP Publishing. 978-0-7354-4037-1/$30.00

be used to improve plant operation significantly in terms of efficiency and lifetime [1-2]. Nowcasting systems consisting of all sky imagers (ASI) can determine current and future irradiance maps required for this optimization. The common principle of such nowcasting systems [e.g. 3-5] is to take photos of the complete sky in which clouds are detected. Using several cameras, the cloud height above the ground can be detected by stereo photography or similar approaches [e.g. 6-7]. This information allows computing cloud shadow maps which can be enhanced to DNI maps with local DNI measurements or clear sky models. The cloud movement is tracked in image series in order to predict future cloud positions and the corresponding DNI maps. For all these evaluation steps, a variety of different methods is available from the literature. In this work, we present the overall evaluation setup which is based on previously published step wise benchmarks for the cloud detection [8], cloud-transmittance [9], cloud-height and cloud-velocity determination [10]. In [9] the overall DNI nowcast quality of the used nowcasting system was validated according to the procedure described in [8]. For a validation period of 2 years (2016 and 2017) and a lead-time of 10 minutes the nowcasting system reached an overall RMSD, MAD, bias, and skill score of 21%, 13%, 5%, and 7%, respectively. This validation campaign was performed at CIEMAT's Plataforma Solar de Almería (PSA). Considering these error metric results, it is necessary to take into account that they show only the overall deviations over the entire data set. However, the nowcasting performance strongly varies with the prevailing weather conditions [11], which makes such overall results less meaningful.

Thus, for the application of ASI nowcasting systems it is essential to know its performance under all relevant atmospheric conditions at the site of interest. Therefore, the ASI based system was tested at five different sites using more than 4.5 years of data. The results of the performance evaluation are analyzed for different atmospheric conditions and presented in this work. To the best of our knowledge this is the by far most extensive validation of an ASI based nowcasting system performed up to now.

ALL SKY IMAGER SYSTEM SETUP

The investigated nowcasting systems use two ASIs, mounted in a distance between 500 m and 2 km from each other. Mobotix Q24 and Q25 of the shelf surveillance cameras with fisheye lenses are utilized as ASIs (see Fig. 1 (left)). Every 30 seconds, new sky images with a 3 MP or 6 MP resolution are taken. An example all sky image of a Q25 ASI is depicted at Fig. 1 (right).

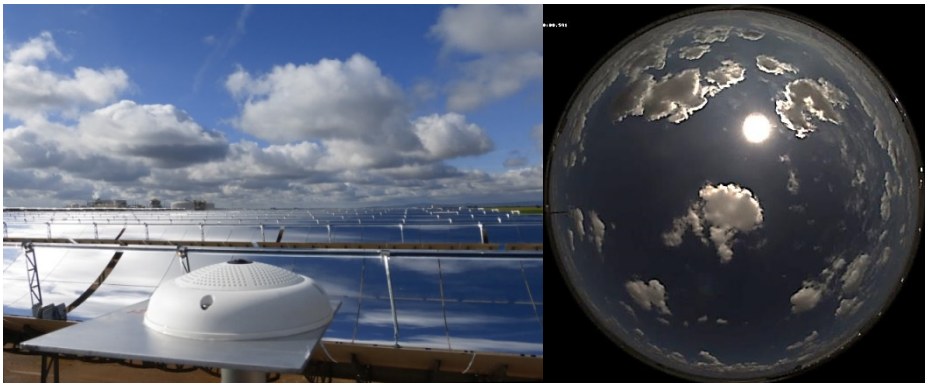

FIGURE 1. (Left) Mobotix Q25 all sky imager at La Africana parabolic trough power plant site (south Spain); (Right) all sky image from Q25 camera.

Table 1 lists the used camera setups for the distinct nowcasting sites. Apart from the ASIs the nowcasting system needs access to DNI measurements from at least one Ground based sensor (e.g. pyrheliometers or rotating shadowband irradiometer). This DNI sensor should be located directly next to one of the ASIs.

TABLE 1. Overview on nowcasting site setups.

Site	Position (central between cameras)	Camera type	Distance between cameras	Used resolution	DNI stations used for validation	DNI stations used by the nowcasting system	Largest distance between DNI station and closest ASI
PSA (Spain)	Latitude: 37.0939° N; Longitude: 2.3590° W	Q24	500 m	3 MP	3	1	520 m
La Africana (Spain)	Latitude: 37.7548° N; Longitude: 5.0576° W	Q25	1910 m	6 MP	2	1	<2 m
Évora (Portugal)	Latitude: 38.5307° N; Longitude: 8.0053° W	Q25	680 m	6 MP	1	1	<5 m
Jülich (Germany)	Latitude: 50.9134° N; Longitude: 6.3874° E	Q25	733 m	6 MP	2	2	210 m
Oldenburg (Germany)	Latitude: 53.1474° N; Longitude: 8.2077° E	Q25	1340 m	6 MP	3	3	3870 m

All five sites use the same image processing software to generate the nowcast. A new set of nowcast results is created with each image series. These nowcast results consist of DNI maps with a spatial resolution down to 5 m for an area of up to 64 km² and lead times up to 15 minutes ahead. Sixteen DNI maps are created for each evaluated image series with lead times from 0 to 15 minutes ahead in one minute steps. Figure 2 illustrates a DNI map within the virtual modeling space with the corresponding cloud models and the marked positions of the ASIs.

One of the key features of the nowcasting system is that each detected cloud is treated as an individual object with distinct attributes such as geolocation, motion vector and transmittance. This enables also a description of the conditions by the nowcasting system during complex but frequent multi-layer conditions. The entire image processing of the nowcasting system is divided into eight distinct processing steps:

1. Clouds are segmented by means of 4-D clear sky library (CSL), accounting for different atmospheric conditions as described in [12] and [8].
2. Geolocation of the clouds is identified by a stereo photography block correlation approach with difference images. Detected clouds are modelled within a 3-D virtual modeling space [10].
3. Cloud motion vectors are identified from three sequential image series by a block correlation approach with difference images from a single ASI [10].
4. Future cloud positions are generated by displacing the cloud models inside a virtual modeling space [13].
5. Cloud transmittance properties are measured only for a few clouds, which shade ground based DNI measurement stations. The remaining cloud objects receive transmittance estimations according to their height, results of a probability analysis with historical cloud height and transmittance measurements as well as recent transmittance measurements and their corresponding cloud height [9].
6. Cloud shadows are projected to a topographical map with ray tracing [13].
7. Shadow projections are combined with the ground based irradiance measurements and the cloud transmittance properties to spatial DNI maps [13].
8. Real time uncertainties of the nowcasting system are determined [14].

The image processing of the nowcasting system is real time capable with an average processing time of 12 seconds per image series, conducted with a common desktop PC (8x3.6GHz Intel Core i9-9900K, 2x16GB DDR4-2666 and PNY Quadro RTX 4000 8GB GDDR6).

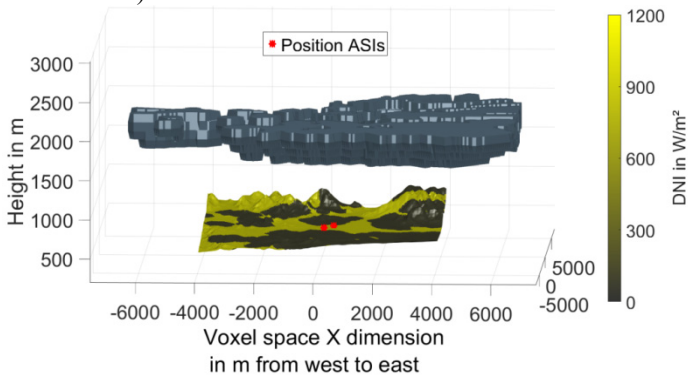

FIGURE 2. Virtual modeling space with cloud models and topographical map around PSA with spatial DNI information.

PERFORMANCE VALIDATION AT FIVE DIFFERENT SITES

In the following section the used validation methodology that considers different atmospheric conditions is presented. Subsequently the results of the validation for distinct sites are presented and discussed.

Description of the Used Validation Method Considering Distinct Atmospheric Conditions

The performance of ASI based DNI nowcast depend on the prevailing atmospheric conditions. Uncertainties will increase during conditions with a high DNI variability and drop under stable conditions with a low variability [14]. Therefore, depending on the selected data set, comparatively high or low error metrics are found. Thus, the comparison of different nowcasting systems and sites is not possible without consideration of the atmospheric conditions. Consequently, in this work the DNI variability is analyzed and classified at any time.

The used DNI variability classification procedure is based on [15] with the adaptations according to [14] using 1 min DNI values over the last 15 minutes. The variability classes describe conditions ranging from clear sky (class 1) to completely overcast (class 8). The higher the class number, the more frequent and the less transparent are the clouds. Table 2 lists a short description for each of the 8 classes.

TABLE 2. Description of DNI variability classes

Class	General description of temporal DNI variability
1	Clear sky conditions with low temporal DNI variability and very high clear sky index
2	Almost clear sky with low temporal DNI variability and high clear sky index
3	Almost clear sky with intermediate temporal DNI variability and high/intermediate clear sky index
4	Partly cloudy with high temporal DNI variability and intermediate clear sky index
5	Partly cloudy with intermediate temporal DNI variability and intermediate clear sky index
6	Partly cloudy with high temporal DNI variability and intermediate/low clear sky index
7	Almost overcast with intermediate temporal DNI variability and low clear sky index
8	Overcast with low temporal DNI variability and very low clear sky index

Each time stamp of the validation data sets is discretized in one of the eight classes. Ground based DNI measurements in 1 min resolution are used for the classification as well as reference signals for the validation.

Mean absolute deviations (MAD) and root mean square deviations (RMSD) discretized over the DNI variability classes are calculated according to the equations 1 and 2.

$$MAD_C = \frac{1}{n_C}\sum_{i_c=1}^{n_C}\left|Y_{i_c} - \hat{Y}_{i_c}\right| \quad (1)$$

$$RMSD_C = \left[\frac{1}{n_C}\sum_{i_c=1}^{n_C}\left(Y_{i_c} - \hat{Y}_{i_c}\right)^2\right]^{0.5} \quad (2)$$

Y_{i_c} represents the reference and $\hat{Y}_{i_c}$ the corresponding nowcasted DNI value from the DNI maps. The index i_c enumerates all time stamps which belong to the same DNI variability class and n_c is the number of time stamps used for the validation. Average error metrics are calculated for sites with more than one reference station.

Presenting Validation Results

The validation data set includes more than 4.5 years of sky images distributed over the five sites. Table 3 lists the used validation periods.

TABLE 3. Validation data set periods for five sites.

	PSA	La Africana	Évora	Oldenburg	Jülich
Validation period	complete years 2016, 2017 and 2018	complete year 2017	42 days between 16.05.2017 and 05.03.2018	86 days between 02.04.2019 and 15.07.2019	80 days between 01.06.2019 and 19.08.2019

Figure 3 shows the DNI variability class distribution corresponding to the validation period for the five sites. Both Spanish sites (PSA and La Africana) show a similar DNI variability class occurrence with around 60% of the data within clear sky conditions (class 1 and 2) and around 20% within overcast conditions (class 7 and 8). Évora the third site located at the Iberian Peninsula shows also a highest occurrence for the clear sky conditions class 1 and 2. The German sites Oldenburg and Jülich are unsurprisingly dominated by highly clouded and often even overcast conditions (class 6, 7 and 8). It must be taken into account, that the PSA and La Africana data sets include at least one or multiple meteorological years, whereas the sites Évora, Oldenburg and Jülich include only subsets of a

meteorological year. The corresponding average DNI discretized over DNI variability classes is listed in Table 4. Significant deviations are visible between the average DNIs from the Iberian Peninsula and Germany when considering all data. However, the average DNIs within the individual classes are quite close to each other. For the remaining deviations within the classes, it should be taken into account that the distinct sites correspond to their local conditions with distinct aerosol and cloud distributions. Furthermore, the different distribution of seasons within the datasets may also have some influence.

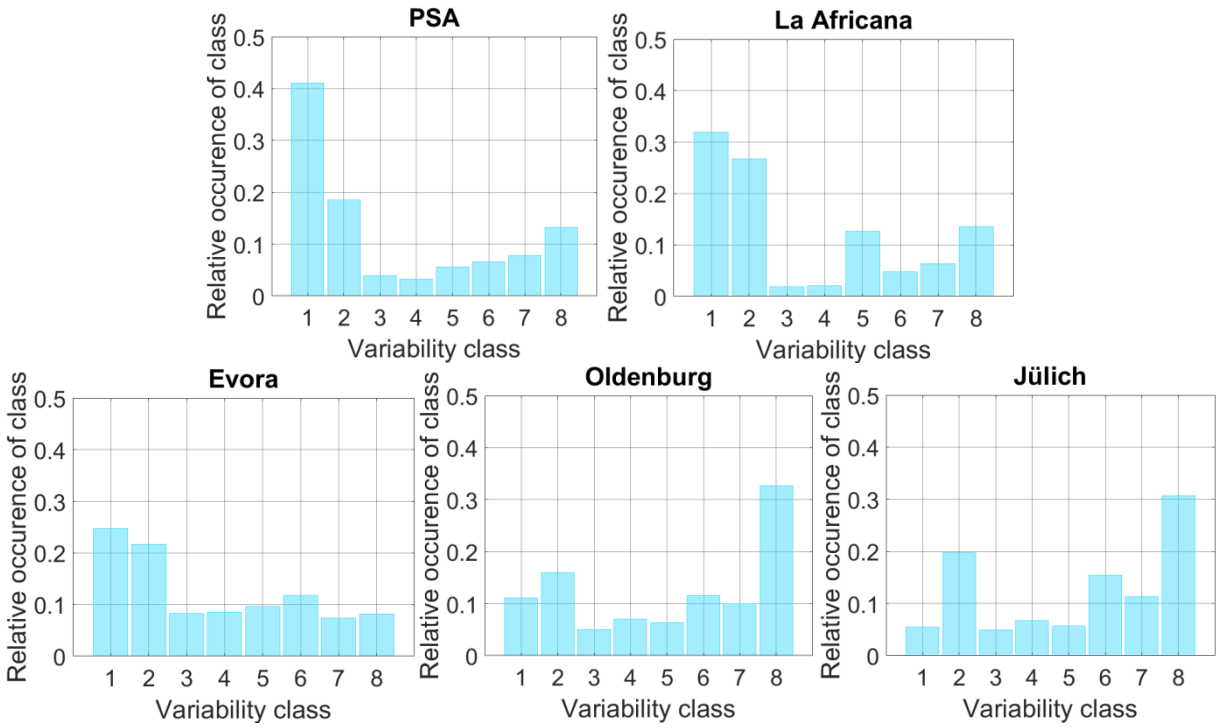

FIGURE 3. Distribution of occurred DNI variability classes over the validation period for the 5 distinct sites.

TABLE 4. Average DNI over the corresponding validation period as measured by one pyrheliometer or rotating shadowband irradiometer at each site discretized over the DNI variability classes.

	Class 1	Class 2	Class 3	Class 4	Class 5	Class 6	Class 7	Class 8	All data
PSA	895 W/m²	719 W/m²	718 W/m²	600 W/m²	506 W/m²	366 W/m²	137 W/m²	11 W/m²	613 W/m²
LaAfricana	908 W/m²	779 W/m²	725 W/m²	600 W/m²	541 W/m²	348 W/m²	162 W/m²	10 W/m²	622 W/m²
Évora	886 W/m²	704 W/m²	725 W/m²	611 W/m²	512 W/m²	398 W/m²	155 W/m²	14 W/m²	592 W/m²
Oldenburg	757 W/m²	735 W/m²	708 W/m²	600 W/m²	522 W/m²	318 W/m²	120 W/m²	3 W/m²	363 W/m²
Jülich	847 W/m²	708 W/m²	646 W/m²	526 W/m²	522 W/m²	296 W/m²	131 W/m²	5 W/m²	345 W/m²

Overall error metrics discretized over DNI variability classes and lead time are given in Fig. 4. As expected, the deviations increase as the lead time increases. Furthermore, a clear dependency is visible between the deviation amplitude and the DNI variability classes. The tendency is for all sites the same. The lowest deviation is found for clear skies (class 1), which is predominantly defined by a low variability and a high clear sky index. As the DNI variability increases also the deviations increase, with the highest deviations for the highly variable conditions (classes 4 and 6). Class 8 for overcast cases represents low DNI variability conditions, which is also reflected by comparatively low deviations. Yet, the deviations are notable higher for class 8 compared to class 1, as the nowcasting system is more prone in overseeing existing clouds rather than to falsely detecting clouds in a clear sky.
A key finding from Fig. 4 is that the spread between the deviations for different sites within a given class is low compared to the spread between different classes in most cases. This corroborates the applicability of the new method to evaluate nowcasting system in a more comparable way.

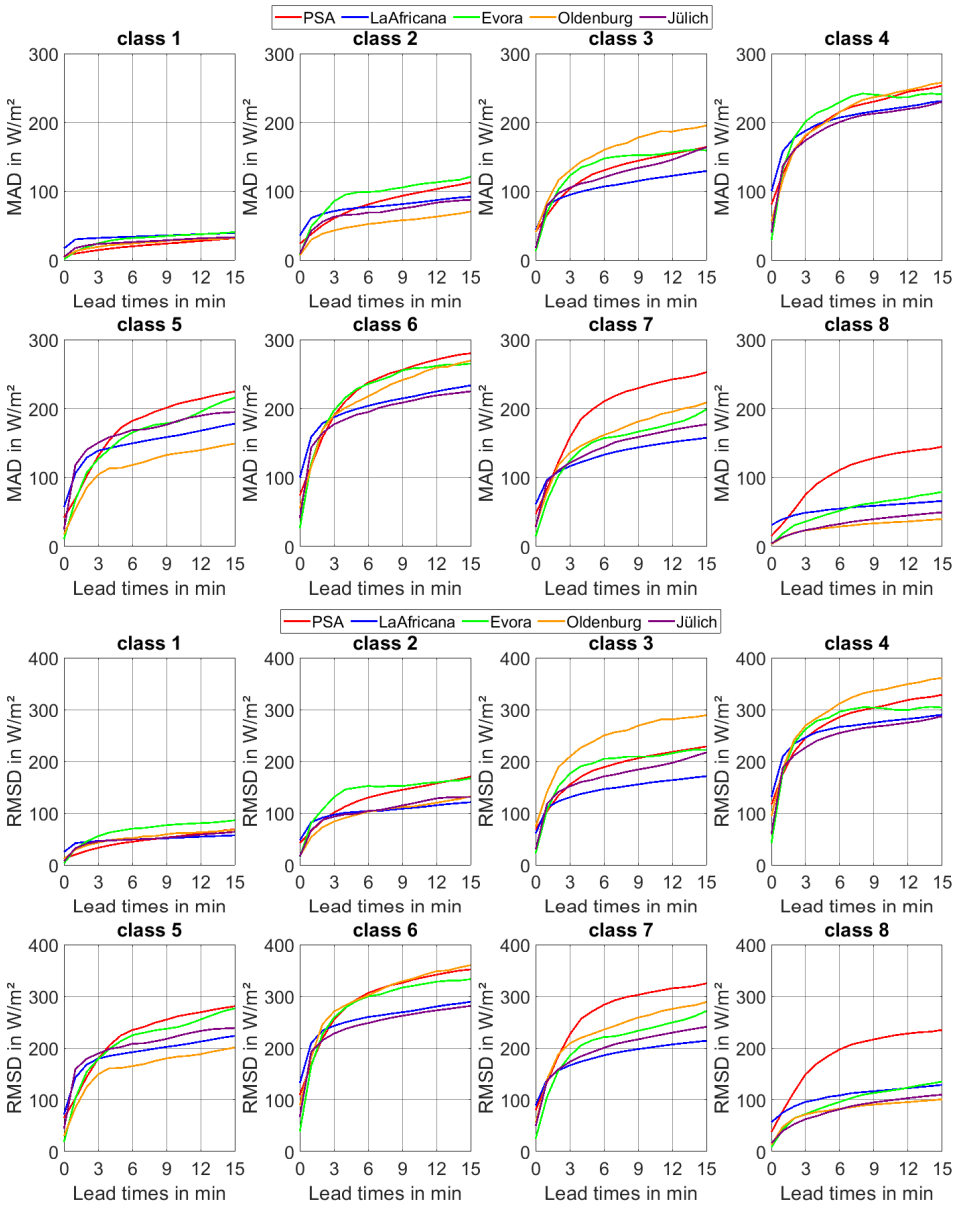

FIGURE 4. Overall MAD and RMSD for the 5 sites distributed over DNI variability classes and lead time.

Depending on the site the DNI variability classes 1, 2 and 8 are the most frequent. As previously stated these are also the classes with the lowest DNI variability and lowest observed deviation. Therefore, these classes may dominate the overall deviations when not considering DNI variability classes. Such overall deviations without consideration of the DNI variability classes can be determined by combining the relative occurrences of the distinct classes from Fig. 3 with the class dependent deviations from Fig. 4. In Fig. 5 it is visible that these overall deviations without consideration of the DNI variability classes are lower than the devaitions in more variable conditions as described by the classes 3 to 7. The nowcast accuracy in less variable cases is higher than for this overall result from Fig. 5.

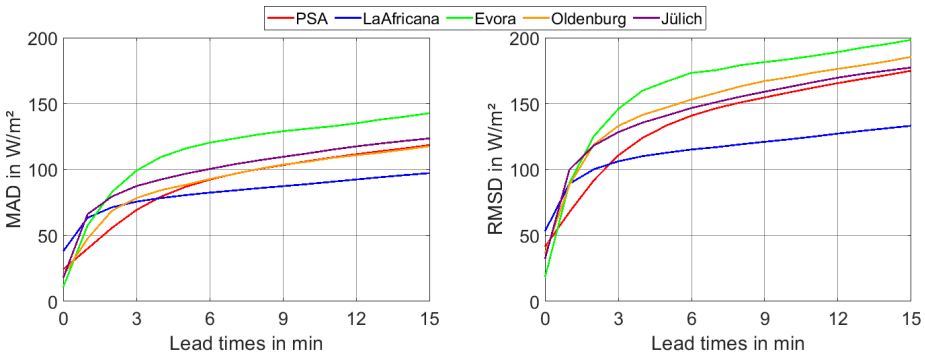

FIGURE 5. Overall MAD and RMSD without consideration of the DNI variability classes for the 5 sites over lead time

From Figure 4 a clear dependency between deviations and DNI variability classes is visible. However, significant fluctuations in performance exist between distinct days from the same site within the same class. This becomes apparent when for each day and class error metrics are calculated individually. Figures 6 to 10 shows the distribution of MAD between all days and classes as box plot describing the 25 and 75 MAD percentiles. Furthermore, the median and mean MAD is shown. The mean MAD resembles the overall MAD from Fig. 4 with some minor deviations. The minor deviations result as each day is equally weighted for the mean MAD. Also visible are considerable deviations in 25 and 75 MAD percentiles between the distinct sites.

These fluctuations in performance between the days as well as between the sites, indicates that the DNI variability classification does not consider all relevant factors that affect the nowcasting performance. This includes the solar zenith angle, cloud height, cloud type and cloud speed [9 & 14].

A further influencing factor on the performance is the used camera set up. Especially the image resolution and the distance between the cameras have a significant impact on the cloud height detection [16], which is one of the key processing steps. Different ideal camera distances exist, depending on the predominant cloud height and image resolution. For example [16] determined an ideal camera distance of 1500 m for the PSA with the 3 MP sky images from Q24 cameras. The used setup at PSA with a camera distance of roughly 500 m is suitable for low layer clouds but will result in increased uncertainties in middle and high layer clouds due to under-sampling effects.

Local meteorological conditions have to be considered as well, when comparing the nowcast performance between distinct sites. For example complex multi-layer conditions are more error prone than single-layer conditions with low layer clouds (e.g. cumulus clouds). Worth mentioning are the conditions at the PSA. The PSA is less than 30 km away from the Mediterranean see and surrounded by the four mountain ranges Sierra de Gádor, Sierra Nevada, Sierra de los Filabres and Sierra Alhamilla. These geographical circumstances often lead to fast changing complex conditions with a scattered cloud cover of multiple layers. Therefore, it comes as no surprise that the strongest fluctuations in nowcast performance are observed for the PSA. The lower camera resolution at PSA compared to the other sites might also contribute to this observation. In the meanwhile the cameras at PSA where replaced by the newer 6 MP models.

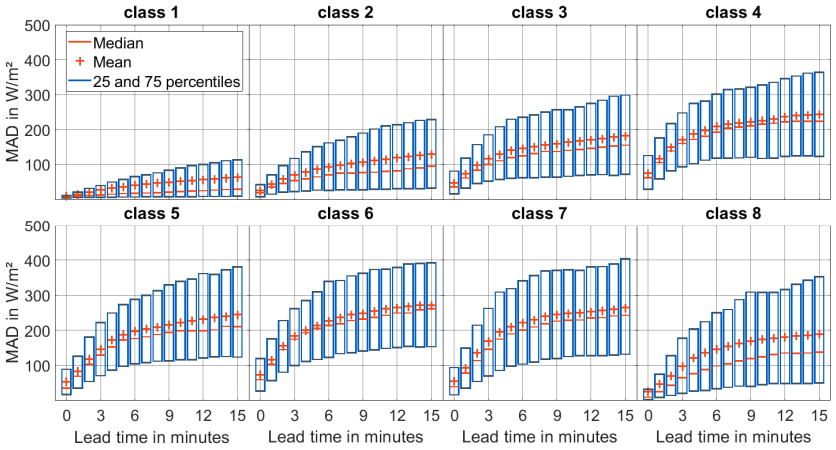

FIGURE 6. Daily MAD distribution at PSA as function of lead time and discretized over DNI variability classes

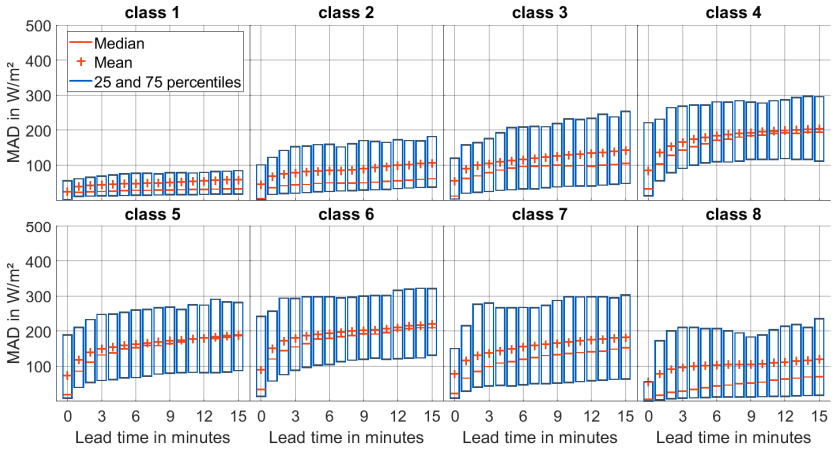

FIGURE 7. Daily MAD distribution at La Africana as function of lead time and discretized over DNI variability classes

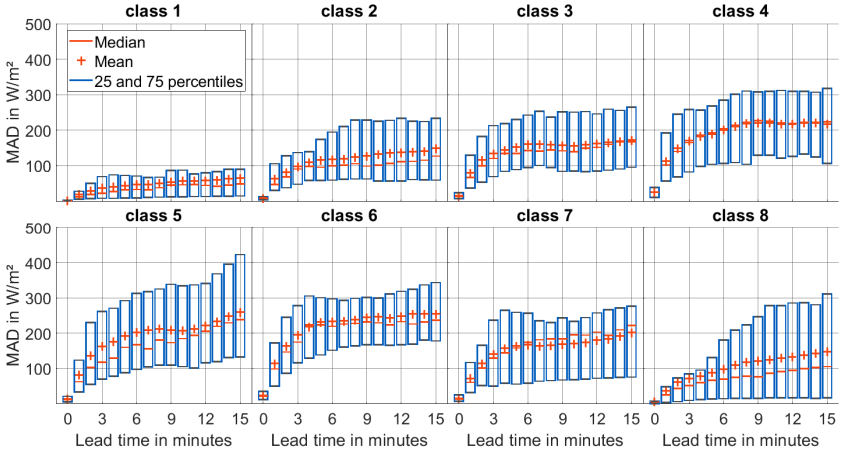

FIGURE 8. Daily MAD distribution at Évora as function of lead time and discretized over DNI variability classes

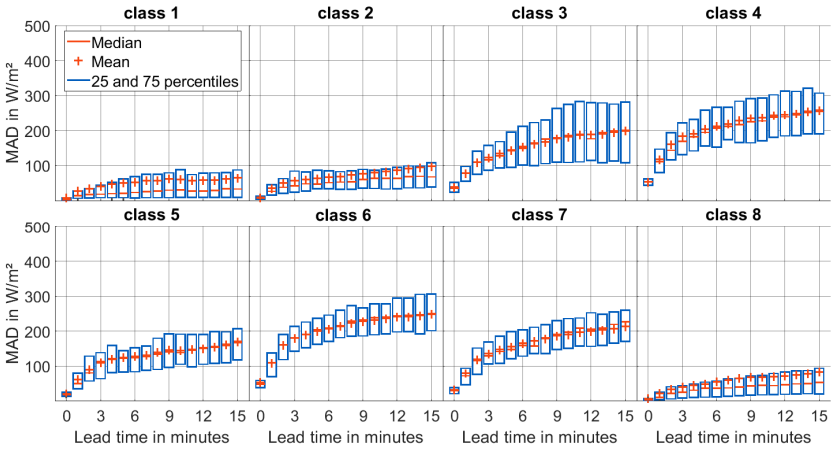

FIGURE 9. Daily MAD distribution at Oldenburg as function of lead time and discretized over DNI variability classes

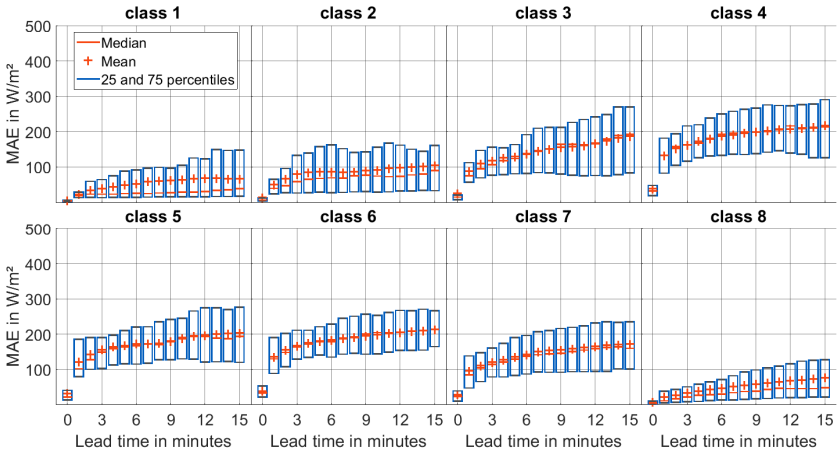

FIGURE 10. Daily MAD distribution at Jülich as function of lead time and discretized over DNI variability classes

CONCLUSION

Nowcasts derived from sky images of more than 4.5 years distributed over 5 sites were validated. All five sites were equipped with two ASIs and used the same image processing software to generate DNI nowcast. DNI maps with an edge length of 8 km and lead times up to 15 minutes ahead were created. The camera set ups differ among the sites with regards to the spacing in between the cameras, from roughly 500 m up to roughly 2 km. Furthermore, Mobotix Q25 cameras with an image resolution of 6 MP were used in four sites, only at PSA Mobotix Q24 cameras with 3 MP resolution were used.

For each site one to three reference ground based DNI sensor were used for the validation. DNI measurements gathered by the ground based sensors were compared to the corresponding DNI nowcasts from the DNI maps. The validation data sets were discretized in eight distinct DNI variability classes from clear sky to overcast, in order to enable a comparison among the different sites. A direct comparison of single error metrics corresponding to the entire data set of each site is not helpful, as the performance of the nowcasts is highly dependent on the chosen data set and the corresponding ambient conditions.

Therefore, MAD and RMSD values were determined as function of the nowcast lead times as well as the DNI variability classes. The same tendency is visible at all sites, with the lowest deviations at conditions with DNI variability class 1, which represents clear sky conditions. All sites show the highest deviations for DNI variability classes 4 and 6. These classes represent a partly clouded sky with a high temporal DNI variability and an intermediate to low clear sky index. Class 6 represents more frequent and less transparent clouds compared to class 4. Under overcast conditions (class 8) the deviations drop again significantly. Similar to class 1 class 8 represents a low temporal DNI variability. Yet, deviations are lower for class 1, as the used nowcasting system is more prone to overseeing existing clouds than to erroneously detecting clouds in a clear sky.

The nowcast validation results for different sites within each class are close to each other compared to the spread of the validation results for different classes. The inclusion of the DNI variability classification represents a clear improvement compared to the state of the art validation methods with singular error metrics without regards to the ambient conditions. The presented method allows the estimation of the overall accuracy of nowcasting systems at a new site if DNI data in 1 min resolution are available.

However, the discretization of the data set in eight temporal DNI variability classes does not take into account all effects that have an influence on the nowcast performance. This can be seen by the fluctuations of the nowcast performances within distinct days. Other effects not taken into account by the DNI variability classes include solar zenith angles and cloud heights. Cloud speed and cloud types are included only implicitly by their impact on solar variability. Furthermore, complex multi-layer conditions are by far more challenging compared to single-layer conditions with low layer clouds. Finally, physical limitations which arise from the used image resolution and distance in between the cameras have to be considered. Therefore, we conclude that the comparison of nowcasting systems at different sites remains a difficult task, even when structurally identical systems are compared and a quantification of the meteorological state of the atmosphere is taken into account (as in this case). When different nowcasting systems are benchmarked against each other, it is recommended to operate all systems in parallel at the same site, to avoid the above mentioned difficulties.

We would like to point out that ASI based nowcasting systems can be used effectively for various applications despite the partly significant uncertainties. According to the studies [2 and 17] the accuracy of the ASI system for lead time 0 min is high enough to allow for a significant yield increase of ~2% for parabolic trough plants by using spatially resolved DNI data. Similar optimizations may also be possible for solar tower plants. We expect further yield improvements when nowcasts (predictions) are implemented for the operation of solar plants.

Furthermore, it is expected that complementary and redundant information/measurements of the atmospheric conditions could increase considerably the accuracy and reliability of nowcasting systems. A network of 34 ASIs and various ground based solar irradiance measurement stations as well as ceilometers is currently being established in and around the city of Oldenburg. All available information within the network are brought together for global horizontal irradiance (GHI), global tilted irradiance (GTI), DNI and photovoltaic feed-in nowcasts with advanced accuracy and extended forecast horizons over an area of roughly 110 km x 100 km [18].

ACKNOWLEDGMENTS

Funding was received by the German Federal Ministry for Economic Affairs and Energy within the WobaS-A project (Grant Agreement 0324307A).

REFERENCES

1. Noureldin, K. Modelling and Optimization of Transient Processes in Parabolic Trough Power Plants with Single-Phase Heat Transfer Fluid. PhD Dissertation, RWTH Aachen, Aachen (Germany). doi: 10.18154/RWTH-2019-10244 (http://publications.rwth-aachen.de/record/771557)
2. Nouri, B., Noureldin, K., Schlichting, T., Wilbert, S., Hirsch, T., Schroedter-Homscheidt, M., Kuhn, P., Kazantzidis, A., Zarzalejo, L.F., Blanc, P., Fernández, J. and Pitz-Paal, R. Optimization of parabolic trough power plant operation using irradiance maps from all sky imagers. Sol. Energy, 198, 434–453. https://doi.org/10.1016/j.solener.2020.01.045 (accepted)
3. Quesada-Ruiz, S., Chu, Y., Tovar-Pescador, J., Pedro, H., Coimbra, C. Cloud tracking methodology for intra-hour DNI forecasting. Sol. Energy 102, 267–275 (2014).
4. Kazantzidis, A., Tzoumanikas, P., Blanc, P., Massip, P., Wilbert, S., Ramirez-Santigosa, L. Short-term forecasting based on all-sky cameras. In Renewable Energy Forecasting; Kariniotakis, G., Ed.; Elsevier Science., 153–178 (2017).
5. Blanc, P., Massip, P., Kazantzidis, A., Tzoumanikas, P., Kuhn, P., Wilbert, S., Schüler, D. and Prahl, C. Short-Term Forecasting of High Resolution Local DNI Maps with Multiple Fish-Eye Cameras in Stereoscopic Mode, AIP conference Proceedings 1850 (2017). doi: 10.1063/1.4984512
6. Kassianov, E., Long, C.N. and Christy, J. Cloud-base-height estimation from paired ground-based hemispherical observations. J. Appl. Meteorol., 44 (8), 1221–1233 (2005). doi: 10.1175/JAM2277.1.
7. Beekmans, C., Schneider, J., Läbe, T., Lennefer, M., Stachniss, C. and Simmer, C. Cloud photogrammetry with dense stereo for fisheye cameras. Atmos. Chem. Phys., 16 (22), 14231–14248 (2016). doi: 10.5194/acp-16-14231-2016.
8. Kuhn, P., Nouri, B., Wilbert, S., Prahl, C., Kozonek, N., Schmidt, T., Yasser, Z., Ramirez, L., Zarzalejo, L., Meyer, A., Vuilleumier, L., Heinemann, D., Blanc, P. and Pitz-Paal, R. Validation of an all-sky imager based nowcasting system for industrial PV plants, Prog Photovolt Res Appl., 1-14 (2017). doi: 10.1002/pip.2968
9. Nouri, B., Wilbert, S., Segura, L., Kuhn, P., Hanrieder, N., Kazantzidis, A., Schmidt, T., Zarzalejo, L., Blanc, P. and Pitz-Paal, R. Determination of cloud transmittance for all sky imager based solar nowcasting. Sol. Energy 181, 251–263 (2019). doi: 10.1016/j.solener.2019.02.004.
10. Nouri, B., Kuhn, P., Wilbert, S., Hanrieder, N., Prahl C., Zarzalejo, L., Kazantzidis, A., Blanc, P. and Pitz-Paal, R. Cloud height and tracking accuracy of three all sky imager systems for individual clouds. Sol. Energy 177, 213–228 (2019). doi: 10.1016/j.solener.2018.10.079
11. Marquez, R. and Coimbra, C. F. Proposed metric for evaluation of solar forecasting models. Journal of solar energy engineering., 135(1)(2013). doi: 10.1115/1.4007496
12. Wilbert, S., Nouri, B., Prahl, C., Garcia, G., Ramirez, L., Zarzalejo, L., Valenzuela, L., Ferrera, F., Kozonek, N. and Liria, J. Application of Whole Sky Imagers for Data Selection for Radiometer Calibration. In: EU PVSEC 2016 Proceedings, 1493–1498 (2016). doi: 10.4229/EUPVSEC20162016-5AO.8.6

13. Nouri, B., Kuhn, P., Wilbert, S., Prahl, C., Pitz-Paal, R., Blanc, P., Schmidt, T., Yasser, Z., Ramirez Santigosa, L. and Heineman, D. Nowcasting of DNI Maps for the Solar Field Based on Voxel Carving and Individual 3D Cloud Objects from All Sky Images, AIP Conference Proceedings. Vol. 2033 (2018). doi:10.1063/1.5067196
14. Nouri, B., Wilbert, S., Kuhn, P., Hanrieder, N., Schroedter-Homscheidt, M., Kazantzidis, A., Zarzalejo, L., Blanc, P., Kumar, S., Goswami, N., Shankar, R., Affolter, R. and Pitz-Paal, R. Real-Time Uncertainty Specification of all Sky Imager Derived Irradiance Nowcasts. Remote Sens. 11(9), 1059 (2019). doi: 10.3390/rs11091059
15. Schroedter-Homscheidt, M., Kosmale, M., Jung, S. and Kleissl, J. Classifying ground-measured 1 minute temporal variability within hourly intervals for direct normal irradiances, Meteorol. Z. (2018). doi: 10.1127/metz/2018/0875
16. Kuhn, P., Nouri, B., Wilbert, S., Hanrieder, N., Prahl, C., Ramirez, L., Zarzalejo, L., Schmidt, T., Yasser, Z., Heinemann, D. and Tzoumanikas, P. Determination of the optimal camera distance for cloud height measurements with two all-sky imagers. Sol. Energy., 179, 74–88 (2019). doi: 10.1016/j.solener.2018.12.038.
17. Nouri, B., Noureldin, K., Schlichting, T., Wilbert, S., Hirsch, T., Schroedter-Homscheidt, M., Kuhn, P., Kazantzidis, A., Zarzalejo, L., Blanc, P., Yasser, Z., Fernández, J. and Pitz-Paal, R. A way to increase parabolic trough plant yield by roughly 2% using all sky imager derived DNI maps. AIP Conference Proceedings. (2020 accepted)
18. Schmidt, T., Heinemann, D., Vogt, T., Blum, N., Nouri, B., Wilbert, S., and Kuhn, P. Energiemeteorologisches Wolkenkameranetzwerk für die hochaufgelöste Kurzfristprognose der solaren Einstrahlung. DACH-Tagung Garmisch Partenkirchen. (March 2019)